Electronic Supplementary Information

Visible-to-ultraviolet (<340 nm) photon upconversion by triplet–triplet annihilation in solvents

Yoichi Murakami,[1,2]* Ayumu Motooka,[1] Riku Enomoto,[1] Kazuki Niimi,[3] Atsushi Kaiho[3] and Noriko Kiyoyanagi[3]

[1] School of Engineering, Tokyo Institute of Technology, 2-12-1 Ookayama, Meguro-ku, Tokyo 152-8552, Japan.

[2] PRESTO, JST, 4-1-8 Honcho, Kawaguchi, Saitama 332-0012, Japan.

[3] Nippon Kayaku Co., Ltd., 3-31-12 Shimo, Kita-ku, Tokyo 115-8588, Japan.

*Corresponding Author: Yoichi Murakami, E-mail: murakami.y.af@m.titech.ac.jp

List of Contents

1. Photostability of visible-to-visible UC in an ionic liquid (Fig. S1)

2. Photostability of UV-UC using biacetyl and PPO in DMF (Fig. S2)

3. Optical absorption spectra of the sensitizer and emitter used in this study (Fig. S3)

4. Information about the solvents used in this study (Table S1)

5. Experimental setup to controllably induce photodegradation (Fig. S4)

6. Calculated dipole moments of the sensitizer and emitter (Fig. S5 and Table S2)

1. Photostability of visible-to-visible UC in an ionic liquid

We have reported several examples of visible-to-visible photon upconversion (UC) by triplet–triplet annihilation (TTA) using ionic liquids as the solvent.[S1–S4] To underpin the motivation of the present study, this supplementary section considers the photostability of such visible-to-visible UC and then the contrasting low photostability of visible-to-ultraviolet UC (UV-UC).

The inset of Fig. S1b shows a photograph of the sample used here, which was prepared and sealed in a quartz tube with a 2×2 mm square cross section on October 30, 2012, according to the procedure described prevously.[S1–S4] This sample was prepared using *meso*-tetraphenyltetrabenzoporphyrin palladium (PdPh$_4$TBP) as the sensitizer and perylene as the emitter with concentrations of 5×10^{-5} M and 2×10^{-3} M, respectively, dissolved in the ionic liquid 1-butyl-2,3-dimethylimidazolium bis(trifluoromethylsulfonyl)amide ([C$_4$dmim][NTf$_2$]). The molecular structures of these materials are shown in Fig. S1a. Since October 2012, this sample has been located on a desktop in our laboratory, where it is exposed to light from fluorescence tubes and weak indirect natural sunlight from outside. This sample still displays similar UC behavior to that at the time of the preparation. The photograph in the inset of Fig. S1b was taken on September 8, 2020, showing the sample was upconverting incident red light (633 nm, ca. 5 mW) into blue emission (around 450–480 nm), demonstrating its long lifetime (>7 years).

Figure S1b illustrates the excellent stability of the UC emission from this sample under continuous irradiation of laser light at 633 nm (3 mW; intensity: ca. 0.6 W/cm^2). This experiment was carried out on February 22, 2020. In contrast, when the sensitizer **1** and emitter **2** used in this article were dissolved in the same ionic liquid at concentrations of 2×10^{-4} and 2×10^{-3} M, respectively (see the Experimental section in the main text), the photostability of the sample was low, as shown by the purple curve in Fig. S1b, which is the same curve as that shown in Fig. 2e of the main text.

This comparison reveals that photodegradation in TTA-UC samples primarily depends on the characteristics of solutes, where molecules used for UV-UC have higher triplet energies than those used for visible-to-visible UC. Furthermore, in the UV-UC explored here, we found that the photostability and UC quantum efficiency (Φ_{UC}) strongly depended on the solvent, which is the subject of the present study.
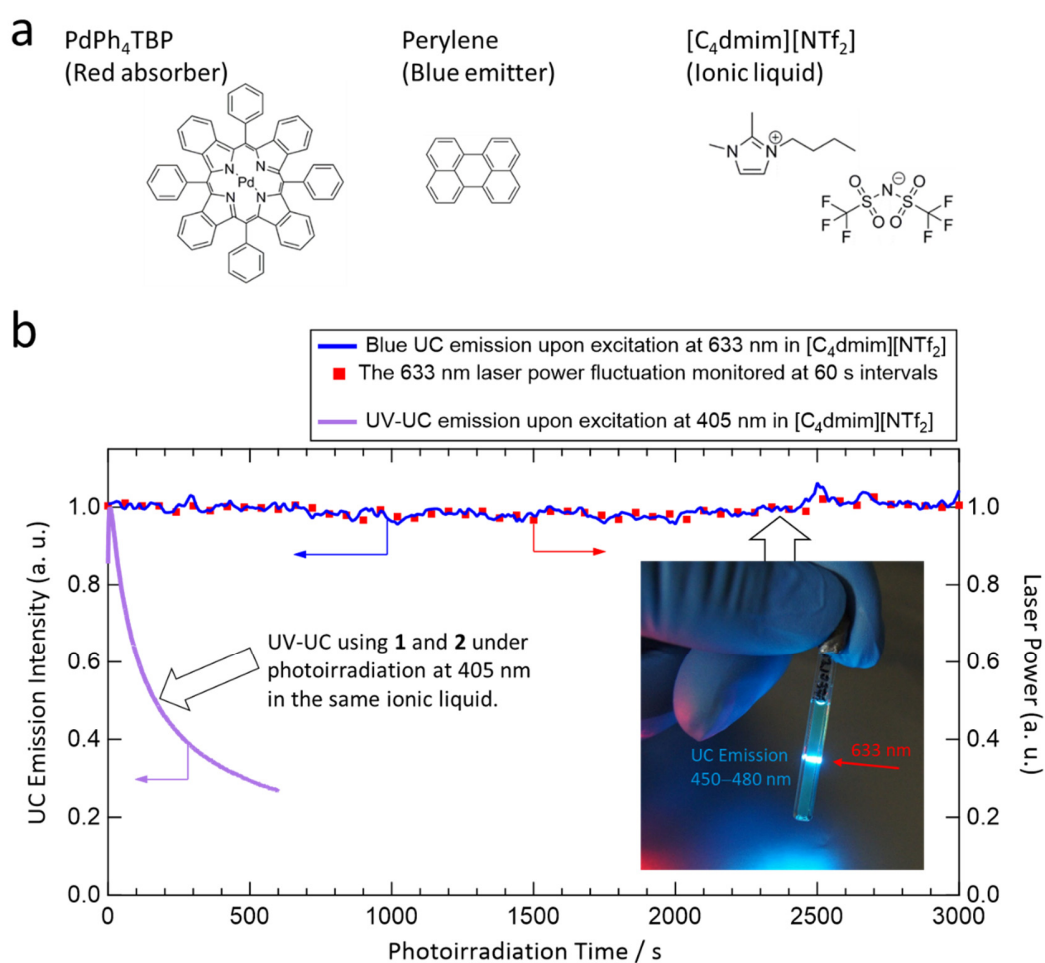
Figure S1. (a) Molecular structures of the sensitizer, emitter, and ionic liquid used here. (b) Temporal UC emission intensity profile acquired from the sample under continuous photoirradiation at 633 nm (blue curve; laser power: 3 mW) along with the simultaneously monitored temporal fluctuation of the laser power (red dots). For comparison, the temporal profile of the UV-UC emission intensity from a sample prepared using the sensitizer **1** and emitter **2** (see the main text for details) in the same ionic liquid under continuous 405-nm irradiation is also shown (purple curve; laser power: 2.2 mW), which is the same curve as that shown in Fig. 2e of the main text. Inset is a photograph of the ionic liquid sample measured here.

2. Photostability of UV-UC using biacetyl and PPO in DMF

To date, several examples of UV-UC using 2,5-diphenyloxazole (PPO), which generates UV emission around 350–400 nm, as the emitter have been reported.[S5–S10] The most representative sensitizer combined with PPO is 2,3-butanedione (biacetyl), as used in the pioneering work by Singh-Rachford and Castellano.[S5] In ref. S5, the authors used benzene as the solvent, presumably to decrease the rate of hydrogen abstraction by the triplet solutes, and reported Φ_{UC} of 0.58%. However, benzene is inappropriate for applications. The other reports that combined biacetyl and PPO used dimethylformamide (DMF) as the solvent.[S7,S9] To support our statements in the Introduction section of the main text, here we present our results for UV-UC samples prepared using biacetyl and PPO in DMF. All the samples used here were deaerated by nine freeze-pump-thaw (FPT) cycles by the method described in the Experimental section of the main text and measured using the same conditions as those used for other samples investigated in this report.

First, we investigated the sample containing only biacetyl at a concentration of 2×10^{-3} M (Fig. S2a–c). Using the setup described in Section 5 of this Supplementary Information, an expanded 405-nm laser beam was irradiated onto the sample under the conditions described therein, which were the same as those used in Fig. 3b and 4a of the main text. After this photoirradiation, the absorbance of biacetyl had disappeared (Fig. S2a). We also measured the temporal changes of the fluorescence spectrum and intensity (Fig. S2b and S2c, respectively) for this sample sealed in a 1×1-mm glass capillary exposed to an excitation power at 405 nm that induced a triplet generation rate of biacetyl of ca. 1.65×10^{-3} M/s (i.e., slightly weaker excitation conditions than those used for Fig. 3a in the main text and Fig. S9 below). The fluorescence quickly diminished during the photoirradiation. These results indicate the low photostability of biacetyl in DMF.

Next, we investigated a sample containing both biacetyl and PPO with concentrations of 2×10^{-3} and 8×10^{-3} M, respectively, which are the same concentrations as those used in ref. S5. The absorption spectrum of this sample is shown in Fig. S2d. Under the same photoirradiation conditions (i.e., triplet generation rate of ca. 1.65×10^{-3} M/s on biacetyl), the UC emission rapidly diminished, almost disappearing within 30 s.

Overall, based on the results presented here, photodegradation in UV-UC is an important issue to investigate and understand. Thus, the issue of photodegradation is not limited to the particular case of **1** and **2** employed in this study. Recently, Lee et al.[S11] also presented a report on this aspect of UV-UC.
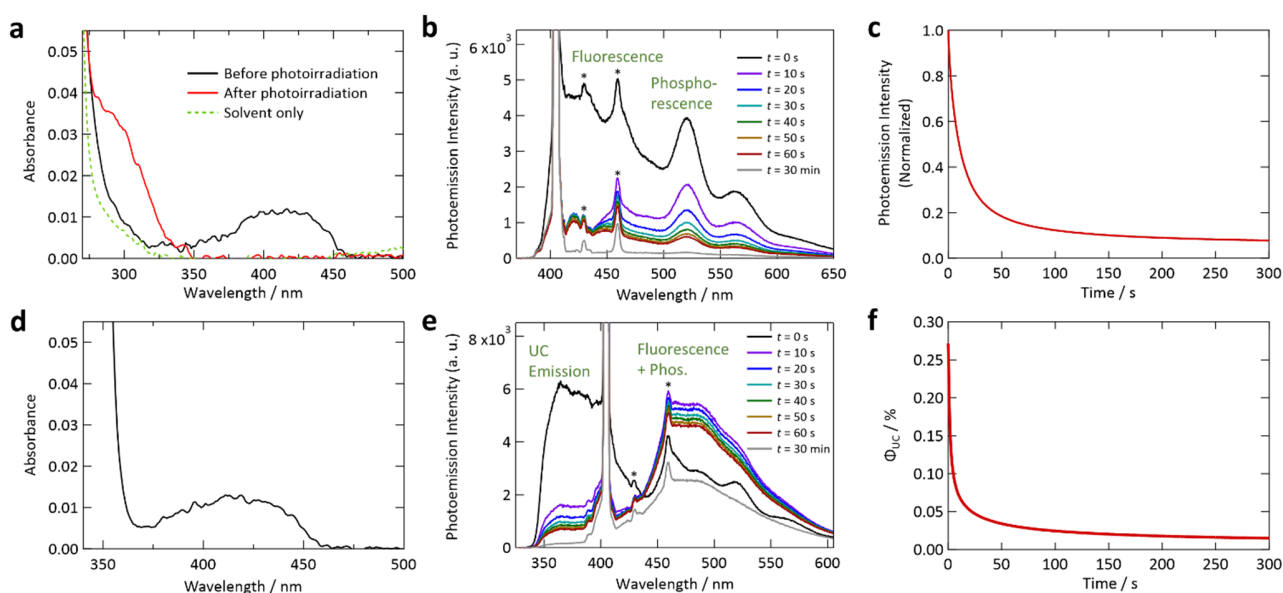

Figure S2. (a) Change of the optical absorption of a sample containing only biacetyl (2×10^{-3} M) in deaerated DMF induced by photoirradiation at 405 nm. (b) Temporal change of the fluorescence spectrum of this sample sealed in a 1×1-mm glass capillary under continuous irradiation at 405 nm and (c) temporal profile of the fluorescence intensity spectrally integrated between 475 and 625 nm. (d) Optical absorption spectrum of a sample containing both biacetyl (2×10^{-3} M) and PPO (8×10^{-3} M) in deaerated DMF. (e) Temporal change of the photoemission spectrum of the sample sealed in a 1×1-mm glass capillary under continuous irradiation at 405 nm and (f) temporal profile of the UC quantum efficiency. In (a) and (d), the optical path length was 1 mm. In (b) and (e), the sharp peaks marked with asterisks were unidentified and may be either Raman scattering from the sample or sidebands from the laser light source.

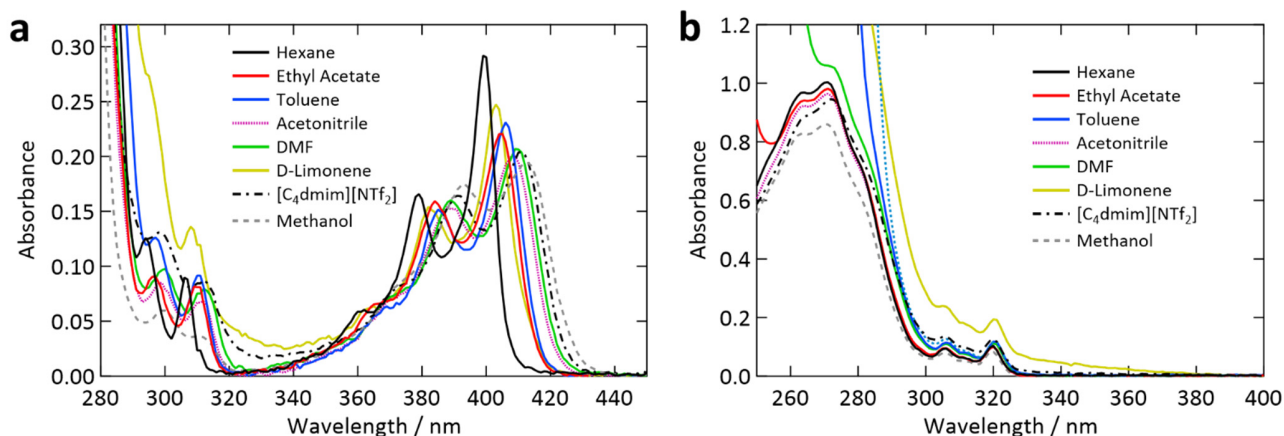## 3. Optical absorption spectra of the sensitizer and emitter used in this study

Figure S3. (a) Optical absorption spectra of the sensitizer **1** and (b) emitter **2** measured in different solvents at concentrations of 2×10^{-4} and 2×10^{-3} M, respectively. The optical path length was 1 mm.

4. Information about the solvents used in this study

Information about the solvents used in this report is summarized in Table S1. The refractive index

values were used to calculate Φ_{UC} in Section 9 of this Supplementary Information.

Table S1. Information about the solvents used in this study

Solvent	Supplier	Purity (Supplier product #)	Refractive index
Hexane	Supelco	≥ 99.7 % (GC) (52750)	1.373[a]
Hexane (reference used in Fig. S8)	TCI	> 99.5 % (GC) (S0278)	
Hexane (reference used in Fig. S8)	Sigma-Aldrich	≥ 95.0 % (GC) (13-0800-5)	
Ethyl Acetate	Wako	99.8+ % (GC) (055-05991)	1.372[a]
Toluene	Wako	99.8+ % (GC) (208-12871)	1.497[a]

Acetonitrile	Wako	99.8+ % (GC) (018-22901)	1.339^a
Dimethylformamide (DMF)	Sigma-Aldrich	≥ 99.90 % (GC) (270547)	1.421^a
D-Limonene	TCI	> 99.0 % (GC) (L0105)	1.474^a
[C_4dmim][NTf_2]	Merck	≥ 98.0 % (HPLC) (490288)	1.435^b
Methanol	Wako	99.9+ % (GC) (139-13995)	1.329^a

[a] From the PubChem website (URL: https://pubchem.ncbi.nlm.nih.gov). All data were collected at the sodium D-line. Temperatures for these values were 30 °C (acetonitrile), 25 °C (D-limonene), 20 °C (ethyl acetate), 25 °C (hexane), 18 °C (mesitylene), 20 °C (methanol), 25 °C (DMF), and 20 °C (toluene).
[b] From ref. S1; at the sodium D-line at 21 °C.

5. Experimental setup to controllably induce photodegradation

Figure S4 illustrates the setup used to controllably induce photodegradation by irradiating an expanded 405-nm laser beam onto almost the entire volume of the sample liquid (2 mL) in a hermetically sealed glass vial (capacity: 6 mL). The liquid height in the vial was ca. 10 mm. The liquid sample was deaerated by conducting FPT cycles just before it was transferred into the hermetically sealed vial; this transfer was promptly carried out inside the vacuum-type SUS glovebox filled with fresh nitrogen gas (see the Experimental section of the main text). As illustrated, the expanded light beam (diameter: ca. 5 mm; power: ca. 22 mW) was incident from the bottom of the vial so that the light was entirely absorbed by the sample. The photoirradiation was continued until each molecule of sensitizer **1** converted to the triplet state 85 times on average. The duration of photoirradiation was chosen assuming that the initial absorbance of **1** at 405 nm did not change during the course of irradiation.
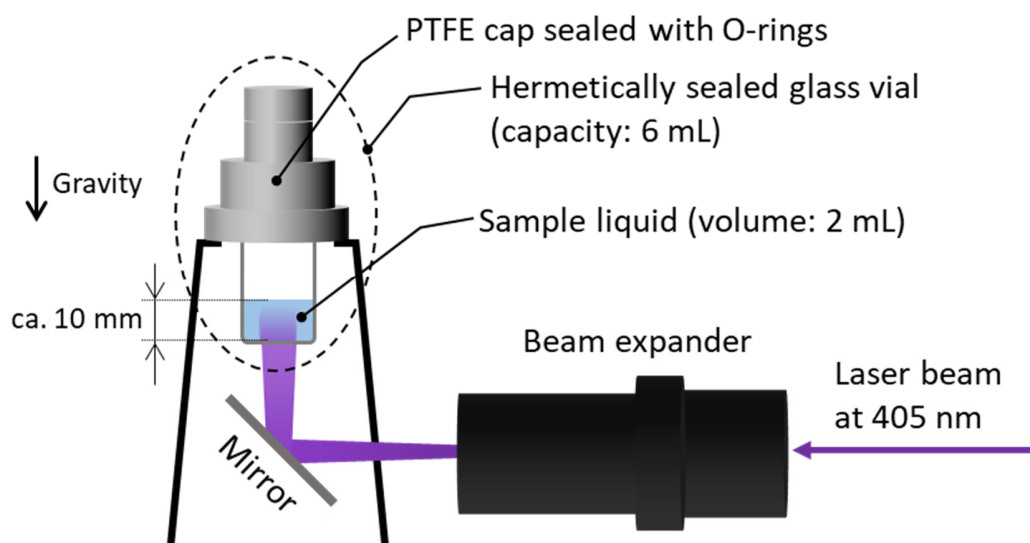
Figure S4. Schematic illustration of the setup to controllably induce photodegradation of a sample liquid.

6. Calculated dipole moments of the sensitizer and emitter

Dipole moments of the sensitizer **1** and emitter **2** were calculated using Gaussian 16® at the B3LYP/6-31G++(d,p) level, as summarized in Table S2. The corresponding graphics are shown in Fig. S5, where the blue arrows represent dipole moment vectors.

Table S2. Calculated dipole moments for the sensitizer **1** and emitter **2**

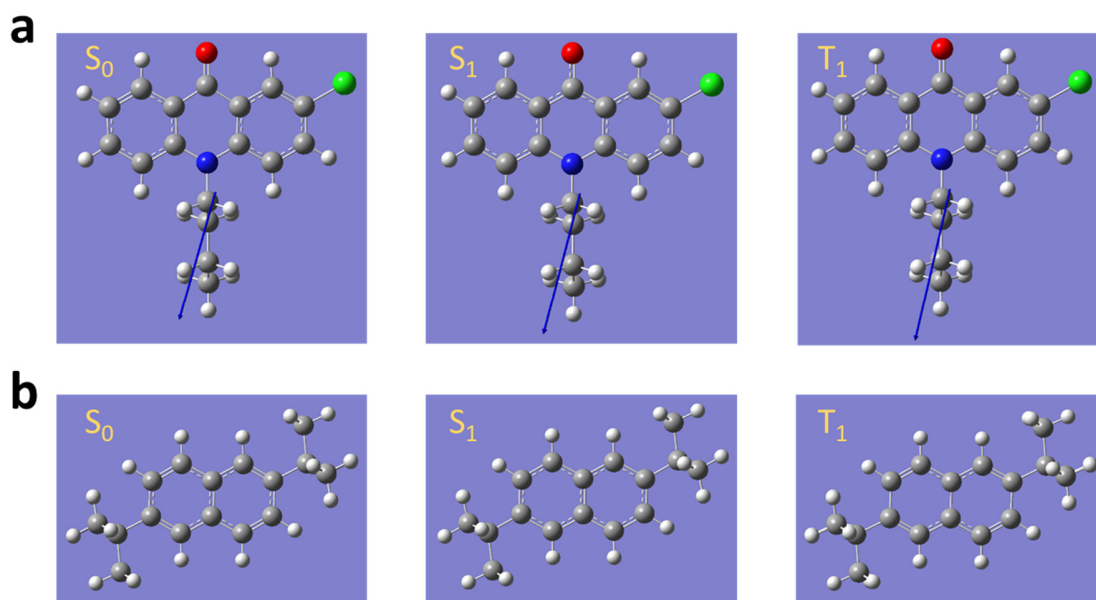|	Electronic State	Dipole Moment (Debye)
Sensitizer **1**	S_0	7.166
	S_1	7.769
	T_1	8.348
Emitter **2**	S_0	0
	S_1	0
	T_1	0

Figure S5. Optimized molecular structures and dipole moments (blue arrows) for (a) sensitizer **1** and (b) emitter **2**.

7. Spectral overlap between emitter fluorescence and sensitizer absorption
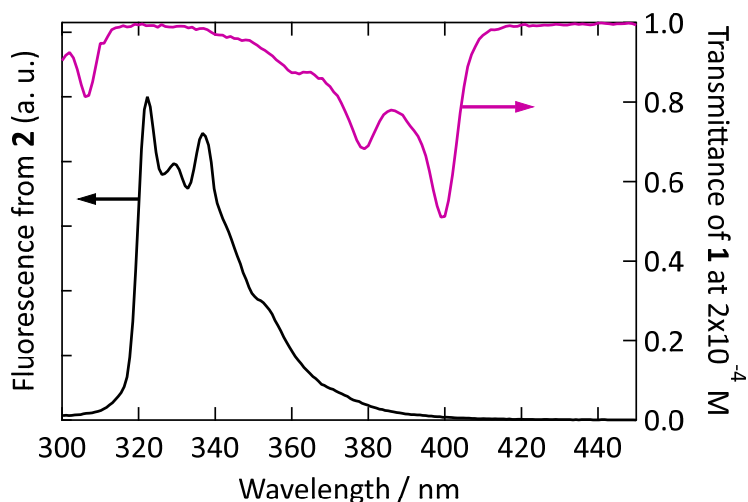

Figure S6. Fluorescence spectrum of **2** (left axis) and transmittance spectrum of **1** (right axis) in hexane generated from the data in Fig. 2a and S3a, respectively. For the transmittance spectrum, the concentration of **1** was 2×10^{-4} M and the optical path length was 1 mm, which are the same conditions as those used to characterize the UV-UC samples.

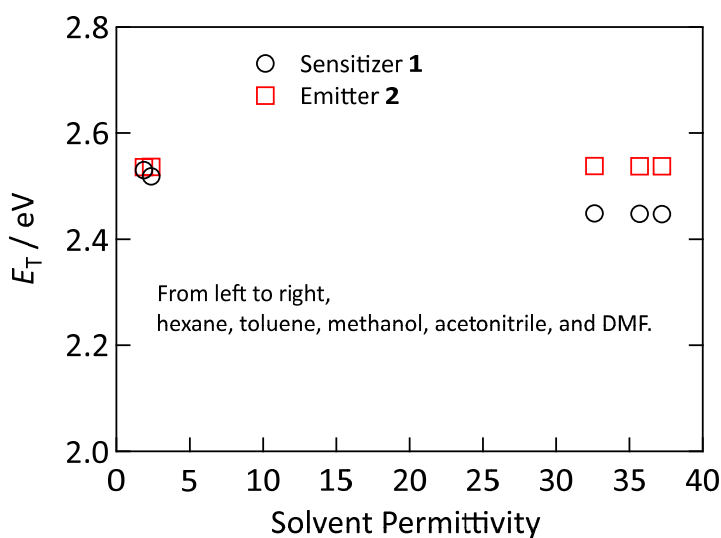## 8. Calculated permittivity dependence of the sensitizer and emitter triplet energies

Figure S7. Calculated triplet energies ($E_T = E(T_1)–E(S_0)$) of **1** and **2** plotted against solvent permittivity. In these calculations, the solvent type was specified in Gaussian $16^®$ where the solvent effect was approximately represented by a polarizable continuum model.

9. Determination of Φ_{UC}

The upconversion quantum efficiency Φ_{UC} (with a defined maximum of 100%) in this article was determined using the following standard relationship.[S12]

$$\Phi_{UC} = 2\Phi_R \left(\frac{1-10^{-A_R}}{1-10^{-A_{UC}}}\right)\left(\frac{I_{UC}^{Em}}{I_R^{Em}}\right)\left(\frac{I_R^{Ex}}{I_{UC}^{Ex}}\right)\left(\frac{h\nu_{UC}}{h\nu_R}\right)\left(\frac{n_{UC}}{n_R}\right)^2 \qquad (S1)$$

Here, Φ_R, A, I^{Em}, I^{Ex}, $h\nu$, and n represent the fluorescence quantum yield of a reference sample, absorbance, photoemission intensity, excitation light intensity, photon energy at the excitation wavelength, and the refractive index of the solvent, respectively. The subscripts "UC" and "R" represent an UC sample and reference, respectively. For the second term on the right-hand side, we used $1-10^{-A}$, which is absorptance, instead of its mathematically approximated form of A (see ref. S12 for further details).

We used a toluene solution of 9,10-diphenylanthracene (concentration: 4×10^{-4} M) deaerated by FPT cycles as the reference sample, which was determined to have Φ_R of 0.940 at the excitation wavelength of 405 nm using our absolute quantum yield spectrometer (Quantaurus-QY, Hamamatsu). The values of n were taken from Table S1. The emission intensity between 310 and 380 nm was used to calculate Φ_{UC}; i.e., the emission between 380 and 405 nm was not used to exclude the tail of the fluorescence and thermally induced UC emission. All photoemission spectra in this report, including those used to determine Φ_{UC}, were corrected by the wavelength-dependent sensitivities of the grating in our monochromator and CCD array detector as reported previously.[S1–S4]

10. Effect of solvent purity on temporal decay profiles of Φ_{UC}

Figure S8 compares temporal decay profiles of Φ_{UC} acquired from three samples prepared under the same conditions using hexane of different purity grades (cf. Table S1). The black curve is the same as that shown in Fig. 2e of the main text. The results reveal that the solvent purity affected the magnitude of Φ_{UC}, especially when low-purity hexane ($\geq$ 95%, in green) was used, but it did not change the qualitative character of the temporal decay profile.

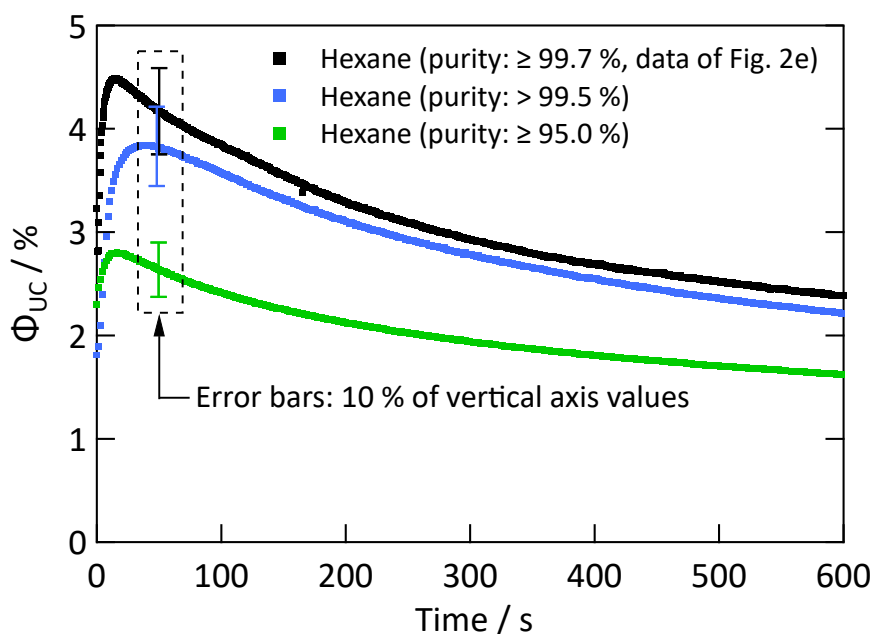

Figure S8. Effect of solvent purity on the decay profiles of Φ_{UC} measured for three samples prepared using hexane with different purity grades (cf. Table S1). The black curve is the data presented in Fig. 2e of the main text.

11. Temporal changes of fluorescence spectra of the sensitizer in the absence of the emitter during photoirradiation in different solvents

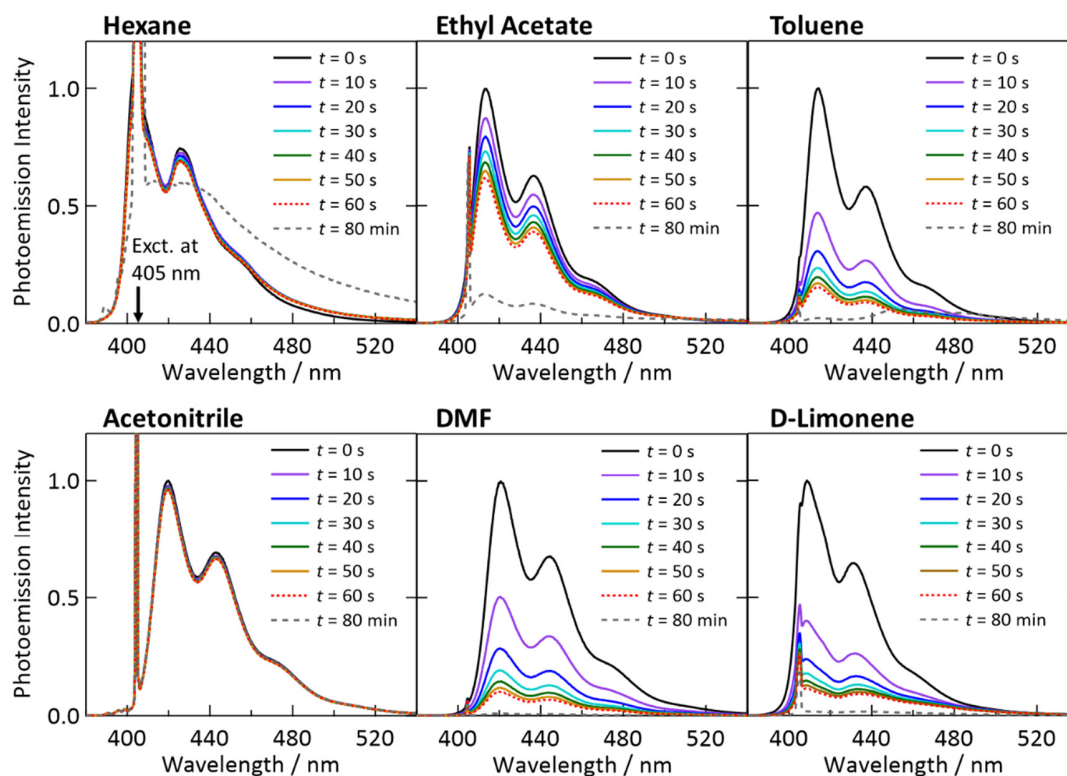**Figure S9.** Temporal decay of the fluorescence spectra of sensitizer **1** acquired under continuous irradiation at 405 nm of samples without emitter **2** sealed in glass capillaries. These results were used to generate the temporal decay curves in Fig. 3a of the main text.

12. Photoirradiation-induced changes of optical absorption spectra of samples containing only the sensitizer in different solvents
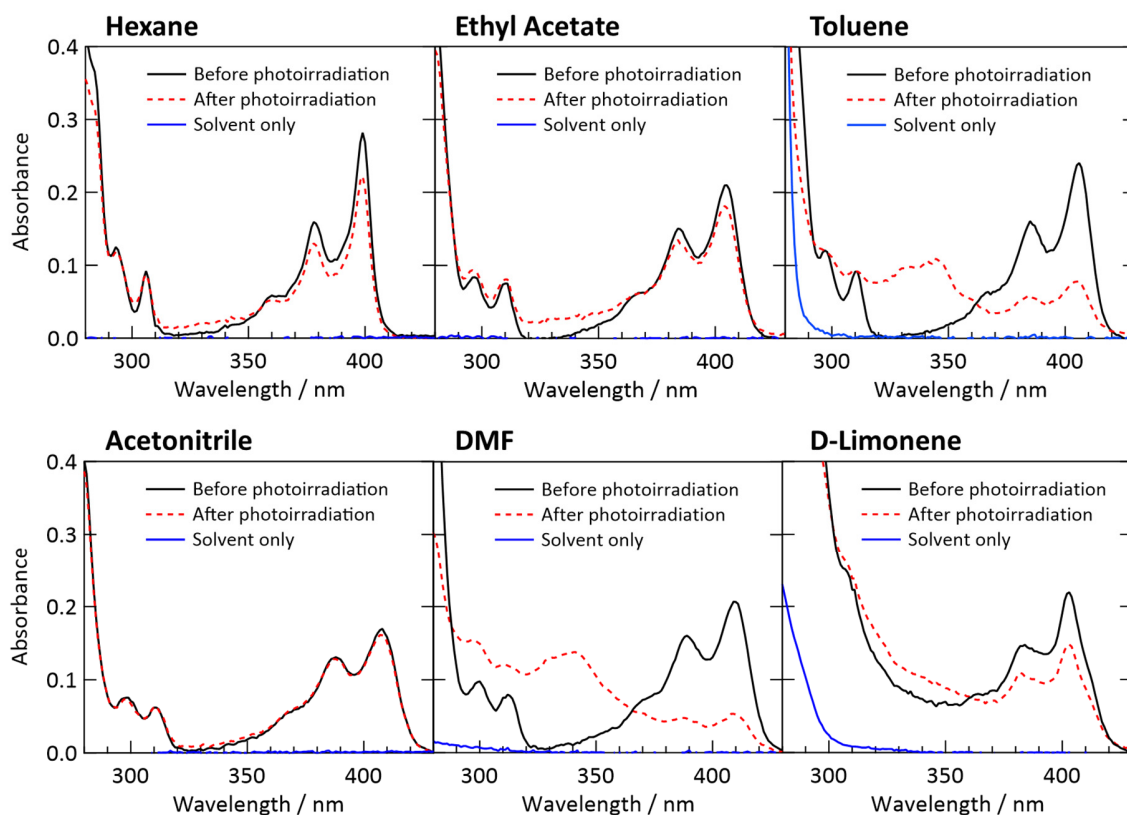
Figure S10. Comparison of optical absorption spectra of samples containing only sensitizer **1** before and after irradiation with 405-nm light. These experiments were carried out using the experimental setup and conditions described in Section 5 of this Supplementary Information. The result for hexane is the same as that shown in Fig. 3b of the main text.

13. Procedure to calculate $k_{\text{sen,degr}}$

Here we describe the procedure used to calculate the photodegradation rate of sensitizer **1** during irradiation with 405-nm laser light from the fluorescence intensity decay curves shown in Fig. 3a of the main text. As mentioned in the main text, these curves were acquired under the same excitation condition; that is, the triplet state of **1** was generated at a rate of ca. 1.9×10^{-3} M/s. Our aim here is to estimate the consumption rate of the sensitizer molecules under this excitation

condition, which is denoted as $k_{sen,degr}$ [mol/(L·s) = M/s]. The consumption of **1** is ascribed to the chemical reaction between **1** in the triplet state and the solvent, as discussed in the main text.

To estimate $k_{sen,degr}$, we fitted the normalized experimental fluorescence intensity decay curves shown in Fig. 3a of the main text with the following double-exponential function

$$I(t) = y_0 + A_1 \exp(-k_1 t) + A_2 \exp(-k_2 t). \tag{S1}$$

Although the real photophysics should be described by more complex kinetic equations, as discussed in the main text, the present procedure is sufficient to obtain values of $k_{sen,deg}$. As illustrated by the fitting curves in Fig. 3a of the main text, eqn (S1) fitted the experimental fluorescence decay curves well in all cases. In eqn (S1), the relation $y_0 + A_1 + A_2 = 1$ holds by definition and the initial condition $I(0) = 1$ corresponds to the initial sensitizer concentration of 2×10^{-4} M.

Then, we employed two reasonable assumptions that (i) the intensity of the fluorescence, which arose from the S_1 state, was proportional to the concentration of intact **1** in the solution, and thus that (ii) both constants k_1 and k_2, although phenomenological, provide quantitative information about the consumption rate of intact **1**. Based on these assumptions, the degradation rate of **1** at $t = 0$ (i.e., when the sensitizer concentration was 2×10^{-4} M), $k_{sen,degr}$, was calculated from the relation

$$k_{sen,degr} = C_0 \times (A_1 k_1 + A_2 k_2). \tag{S2}$$

$$\left[\frac{mol}{L \cdot s}\right] \qquad \left[\frac{mol}{L}\right] \qquad \left[\frac{1}{s}\right]$$

Here, C_0 is the initial sensitizer concentration of 2×10^{-4} M. Table S3 summarizes the fitting results and calculated values of $k_{sen,degr}$ for **1** in different solvents.

Table S3. Results of fittings by eqn (S1) and $k_{\text{sen,degr}}$ calculated from eqn (S2) for **1** in different solvents.

Solvent	A_1	k_1 / s	A_2	k_2 / s	$k_{\text{sen,degr}}$ / M s^{-1}
Hexane	0.06535	0.007170	0.04374	0.07327	7.347×10^{-7}
Ethyl Acetate	0.3550	0.003677	0.3449	0.03024	2.347×10^{-6}
Toluene	0.1976	0.01187	0.7112	0.1066	1.563×10^{-5}
Acetonitrile	0.02419	0.01081	0.0234	0.07627	4.092×10^{-7}
Dimethylformamide (DMF)	0.1262	0.01077	0.8627	0.08417	1.479×10^{-5}
D-Limonene	0.1467	0.01125	0.7895	0.1212	1.947×10^{-5}

14. Plots of $k_{\text{sen,degr}}$ against ionization energy and electron affinity

The results in Fig. 3d of the main text were presented based on HOMO and LUMO levels. Although the representation using HOMOs and LUMOs is easy to understand intuitively, in general, the quantitative reliability of orbital energy levels is affected by the choice of the basis set and level of theory used in the calculation. (In this report, all quantum-chemical calculations were performed using Gaussian 16$^®$ at the B3LYP/6-31G++(d,p) level.)

To alleviate this concern, use of the ionization energy (IE) and electron affinity (EA), which physically correspond to HOMO and LUMO energies, respectively, can enhance the quantitative reliability of analysis. This is because both IE and EA are calculated based on the total energy of the molecule considered, which means they are less affected by the choice of the basis set and calculation level than calculated HOMO and LUMO energies. Specifically, IE can be calculated by subtracting the energy of the neutral ground-state species from that of the radical cation species, and EA can be calculated by subtracting the energy of the radial anion species from that of the

neutral ground-state species. Here, energies of the radial cation and radical anion were calculated using the molecular structure of the neutral ground-state species (i.e., vertical assumption).

Figure S11 shows plots of $k_{sen,degr}$ against the difference between the IEs (left, corresponding to $\Delta|$HOMO$|$) of **1** and the solvents and that between the EAs (right, corresponding to $\Delta|$LUMO$|$) of **1** and the solvents. We observed that $k_{sen,degr}$ was correlated with the difference of IEs, whereas no correlation of $k_{sen,degr}$ with the difference of EAs was found, supporting the results in Fig. 3d of the main text.
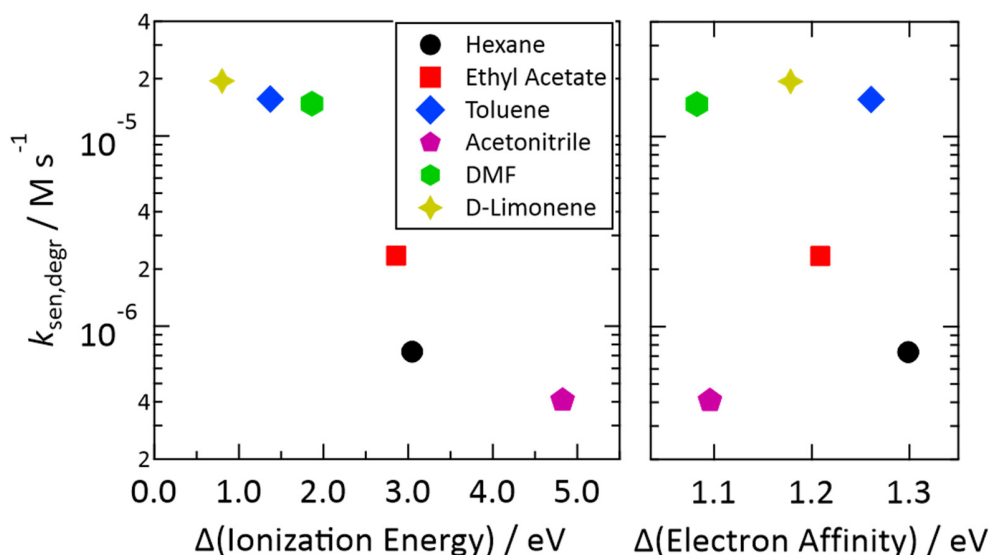

Figure S11. Degradation rates of the fluorescence intensities determined from the results in Fig. 3a of the main text, plotted against the difference between the ionization energies of **1** and the solvents (left) and the difference between the electron affinities of **1** and the solvents (right). See also Fig. 3d in the main text.

15. Procedure to calculate $\Phi_{sen,rxn}$

The experiments in Fig. S10 above were carried out by the method described in Section 5 of this Supplementary Information. As written therein, the photoirradiation time for each experiment was chosen assuming that the absorbance of **1** at 405 nm did not change during photoirradiation. To

estimate the reaction quantum yield of the T_1 state of **1** and solvent ($\Phi_{sen,rxn}$) from the results of Fig. S10, the effect of using this assumption needs to be corrected. The details of this procedure are presented below.

First, we introduce the molar quantity of the intact sensitizer in the test vial of Fig. S4, denoted as z, which is a function of time t and thus $z(t)$. The initial value $z(0)$ is $(2 \times 10^{-4}$ mol/L$) \times (2 \times 10^{-3}$ L$) = 4 \times 10^{-7}$ mol. We also introduce the absorbance of the sample liquid with an optical path length of 10 mm (cf. Fig. S4) at a wavelength of 405 nm, denoted as A, which is also a function of time and thus $A(t)$. The initial value $A(0)$ was calculated from A_{405nm} in Table 1 of the main text. Using these parameters, $z(t)$ and $\Phi_{sen,rxn}$ were related with each other by

$$N_A \frac{dz}{dt} = -G_{ph}(1 - 10^{-A})\Phi_{T,sen}\Phi_{sen,rxn}. \tag{S3}$$

Here, N_A is the Avogadro constant, G_{ph} is the number of photons at 405 nm incident to the sample per unit time, and $\Phi_{T,sen}$ is the triplet quantum yield of **1** listed in Table 1 of the main text. Furthermore, there is a relationship of

$$A = \sigma z \Longleftrightarrow z = \frac{A}{\sigma}, \tag{S4}$$

where σ is a proportionality constant with a unit of mol^{-1}. σ depends on the solvent and was in the range of ca. 1.6–6×10^6 mol^{-1} in the present study. By substituting eqn (S4) into eqn (S3), we obtain

$$\frac{dA}{dt} = -\gamma(1 - 10^{-A}) \tag{S5}$$

where

$$\gamma = \frac{G_{ph}\Phi_{T,sen}\sigma}{N_A}\Phi_{sen,rxn}. \tag{S6}$$

On the right-hand side of eqn (S6), all parameters except $\Phi_{sen,rxn}$ are known. Thus, the parameter γ in eqn (S5) is an undetermined constant that is the function of only $\Phi_{sen,rxn}$.

From the experimental results in Fig. S10 for samples containing only the sensitizer **1**, the initial and final absorbance values at 405 nm are known for each solvent. Eqn (S5) describes the temporal decrease of A under the continuous incidence of G_{ph} photons to the sample. This differential equation was analytically solved using the online mathematical service of Wolfram|Alpha.[S13] Finally, by applying the known parameters, the values of $\Phi_{sen,rxn}$ were calculated to be 2.7×10^{-3} (hexane), 2.3×10^{-3} (ethyl acetate), 8.7×10^{-3} (toluene), 7.3×10^{-4} (acetonitrile), 1.1×10^{-2} (DMF), and 4.6×10^{-3} (D-limonene), as plotted in Fig. 3e of the main text.

16. Photoirradiation-induced changes of optical absorption spectra of samples containing both the sensitizer and emitter in different solvents
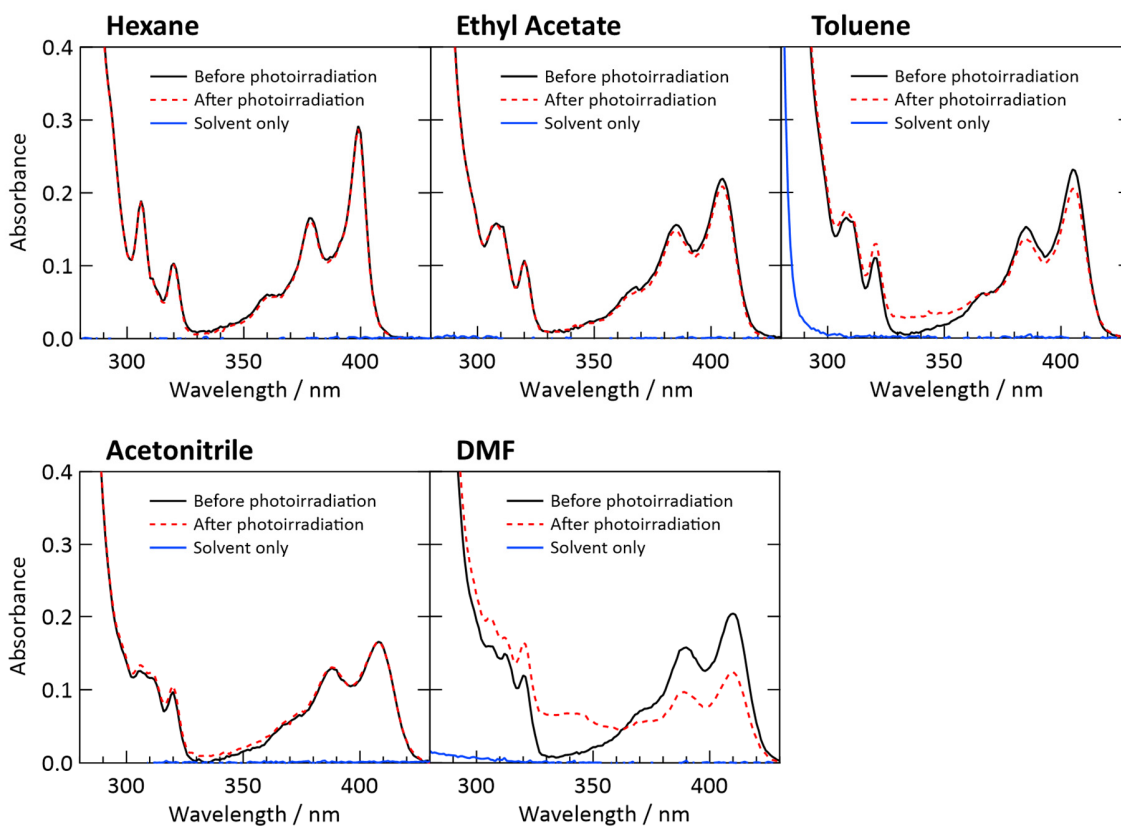

Figure S12. Comparison of optical absorption spectra of samples containing both sensitizer **1** and emitter **2** before and after irradiation with 405-nm light. These experiments were carried out using the experimental setup and conditions described in Section 5 of this Supplementary Information. The results for hexane are the same as those shown in Fig. 4a of the main text.

17. Temporal changes of fluorescence spectra of the sensitizer in the presence of the emitter during photoirradiation in different solvents
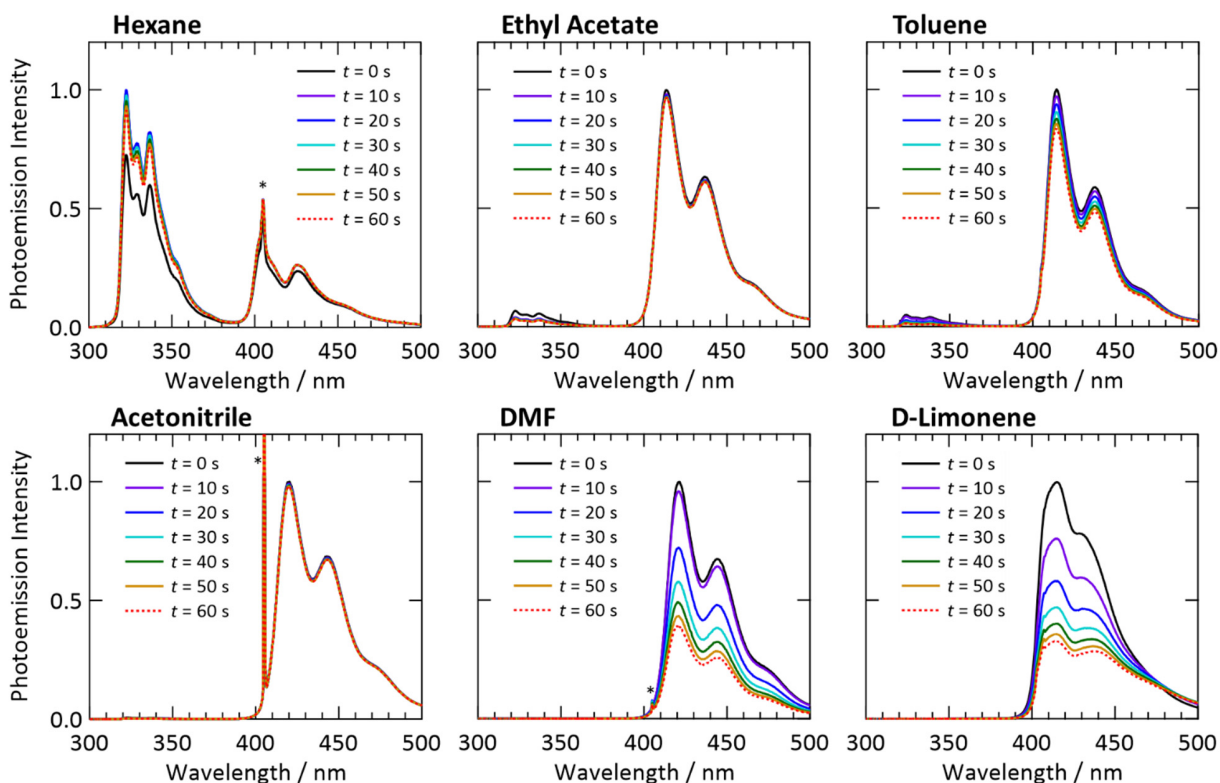
Figure S13. Temporal decay of the fluorescence spectrum of sensitizer **1** acquired under continuous irradiation of 405-nm laser light for samples also containing emitter **2** sealed in glass capillaries. Asterisks indicate peaks from the laser light at 405 nm. See also Fig. 4b in the main text for the spectra of the sample with hexane in a different time range of 0−80 min.

18. Effect of photoirradiation on the triplet lifetime of the emitter

Here, to confirm the postulation of our theoretical model described in the main text, the photoirradiation-induced generation of quenching species is investigated. To do this, we used the experimental setup and photoirradiation conditions described in Section 5 of this Supplementary Information to controllably induce photodegradation of samples before measuring triplet lifetimes.

We measured and compared the triplet lifetimes (τ_T) of the emitter **2** in three samples prepared by different methods described below. All these samples used hexane, which is the representative

solvent in this report. τ_T was obtained by doubling the single-exponential decay time constant of the UC emission (τ_{UC}) acquired with a weak pulsed excitation where TTA is not a dominant process of triplet depopulation; i.e., $\tau_T \cong 2\tau_{UC}$.[S2] The measurements were carried out using nanosecond light pulses as described in the Experimental section of the main text.

The first sample was a normal (fresh) sample without prior photoirradiation, deaerated by FPT cycles and sealed in a glass capillary. The UC emission decay curve of this samples is indicated by black dots in Fig. S14 and its τ_T was found to be 114 μs. The second sample (control sample #1) was prepared by the following procedure. A solution containing only the sensitizer was deaerated by FPT cycles and then photoirradiated using the setup in Fig. S4. The fresh emitter was dissolved in the solution and then it was deaerated again by FPT cycles before being sealed in a glass capillary. The decay curve for control sample #1 is shown by blue dots in Fig. S14, exhibiting τ_T of 12.5 μs. The third sample (control sample #2) was prepared by photoirradiation of the normal deaerated sample containing both the sensitizer and emitter first, and then deaerated again by FPT cycles before being sealed into a glass capillary. The emission decay curve for control sample #2 is indicated by green dots in Fig. S14, showing τ_T of 63.8 μs. These results reveal that photoirradiation shortened τ_T of the emitter, which supports our postulation in the proposed model that photoirradiation generates species that quench the triplet species in the sample.
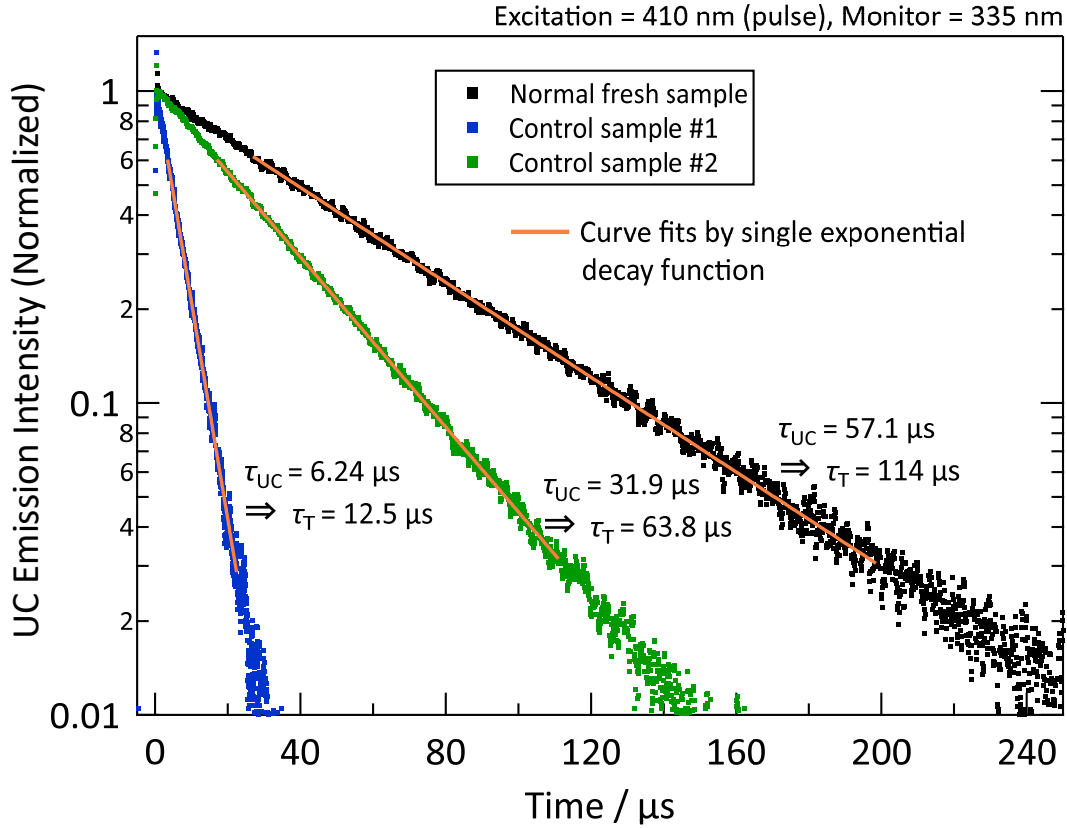
Figure S14. UC emission decay curves acquired for three samples prepared by different methods, which are the normal deaerated sample with fresh sensitizer and emitter (black dots), the sample prepared using the photoirradiated sensitizer solution to which fresh emitter was added and deaerated again (blue dots), and the sample first photoirradiated in the presence of both sensitizer and emitter and then deaerated again (green dots). These intensity decay curves were acquired using weak pulsed excitation at 410 nm and monitored at 335 nm. All these curves were fitted well by single-exponential decay functions, as shown by the orange lines. Determined values of τ_{UC} and τ_T are shown near each curve.

19. Calculation details of our theoretical model

Here we describe in detail the method used to calculate the temporal UC emission curves, examples of which are shown in Fig. 4c of the main text, from the results of our kinetic model

$$k_{\text{diff}}[E^*]^2 + \{k_T + k_{\text{diff}}([\varepsilon] + [Q])\}[E^*] - \left(\frac{[E]}{[E]+[Q]+[\varepsilon]}\right)\Gamma = 0, \tag{S7}$$

which is eqn (10) in the main text. In eqn (S7), [E*] is the concentration of the triplet emitter; hereafter, we use the symbol x in place of [E*]. Because eqn (S7) is a quadratic equation, it can be solved as

$$x = \frac{-k_T - k_{\text{diff}}([\varepsilon]+[Q]) + \sqrt{\{k_T + k_{\text{diff}}([\varepsilon]+[Q])\}^2 + 4k_{\text{diff}}\Gamma\{[E]/([E]+[Q]+[\varepsilon])\}}}{2k_{\text{diff}}}. \tag{S8}$$

Here, the sign just before the square-root term in the numerator must be '+' to be physically valid. The magnitude of the UC emission intensity I_{UC} at time t ($I_{\text{UC}}(t)$), the determination of which is the purpose of this analysis, is obtained by

$$I_{\text{UC}}(t) = \alpha x^2, \tag{S9}$$

where α is an instrumental constant that can be later eliminated by appropriate normalization. The values of k_T and k_{diff} in eqn (S8) were determined from the time-resolved UC emission measurements (e.g., Fig. S14) and eqn (1) in the main text, respectively.

Once we calculate the temporal progressions of [E], [Q], and [ε] after the onset of photoirradiation for $t > 0$, the function $I_{\text{UC}}(t)$ can be obtained from eqn (S9). The initial values (at $t = 0$) for [E], [Q], and [ε] are 2×10^{-3} ($\equiv$ [E$_0$]), Q$_0$, and 0 M, respectively. Here, Q$_0$ is an unknown constant that will be treated as an adjustable parameter in the later computation. The time progressions of these parameters are expressed by the following equations:

$$[E] = [E_0] - k_{\text{emi,rxn}} \int_{s=0}^{s=t} x\,ds \tag{S10}$$

$$[Q] = [Q_0] - \Phi_{\text{Q,rxn}} k_{\text{diff}} \int_{s=0}^{s=t} [Q]x\,ds \tag{S11}$$

$$[\varepsilon] = [E_0] - [E] - \Phi_{\varepsilon,\text{rxn}} k_{\text{diff}} \int_{s=0}^{s=t} [\varepsilon]x\,ds \tag{S12}$$

These integral equations can readily be computed by iterating numerical loops in which an infinitesimal time step Δt is taken in each loop to calculate the temporal evolution for $t \to t + \Delta t$. In the actual computation, we introduced an additional variable $[\varepsilon_{\text{disappear}}]$, which is the cumulative amount of species ε deactivated by the process described by eqn (4) in the main text. Overall, the set of numerical relations used for the computation is:

$$[E(t + \Delta t)] = [E(t)] - k_{\text{emi,rxn}} x \Delta t \qquad (S13)$$

$$[Q(t + \Delta t)] = [Q(t)] - \Phi_{Q,\text{rxn}} k_{\text{diff}} [Q(t)] x \Delta t \qquad (S14)$$

$$[\varepsilon_{\text{disappear}}(t + \Delta t)] = [\varepsilon_{\text{disappear}}(t)] + \Phi_{\varepsilon,\text{rxn}} k_{\text{diff}} [\varepsilon(t)] x \Delta t \qquad (S15)$$

$$[\varepsilon(t + \Delta t)] = [E_0] - [E(t + \Delta t)] - [\varepsilon_{\text{disappear}}(t + \Delta t)] \qquad (S16)$$

By iterating the numerical loop while increasing the time by Δt for each loop, the values of $[E(t)]$, $[Q(t)]$, and $[\varepsilon(t)]$ are obtained, from which the temporal curve of $I_{\text{UC}}(t)$ is generated. In the computation, the generated temporal curve was fitted to the experimentally acquired curve by treating Q_0, $k_{\text{emi,rxn}}$, $\Phi_{Q,\text{rxn}}$, and $\Phi_{Q,\text{rxn}}$ as adjustable parameters; the values of $k_{\text{emi,rxn}}$ in Fig. 4d of the main text were obtained from this fitting procedure. As mentioned in the main text, the fittings yielded Q_0 of 5×10^{-4} M or lower in this study, which is equivalent to a molar fraction of 0.005% or lower. This is a trace amount and thus does not contradict the certified purities of the solvents (cf. Table S1).

20. Plots of $k_{emi,rxn}$ against ionization energy and electron affinity

Similar to Section 14 of this Supplementary Information, in Fig. S15 below, we plotted $k_{emi,rxn}$ against the difference between the IEs of **2** and the solvents (left) and that between the EAs of **2** and the solvents (right). As seen, $k_{emi,rxn}$ is correlated with the difference of EAs, whereas no correlation of $k_{emi,rxn}$ with the difference of IEs is found, supporting the results in Fig. 4d of the main text.
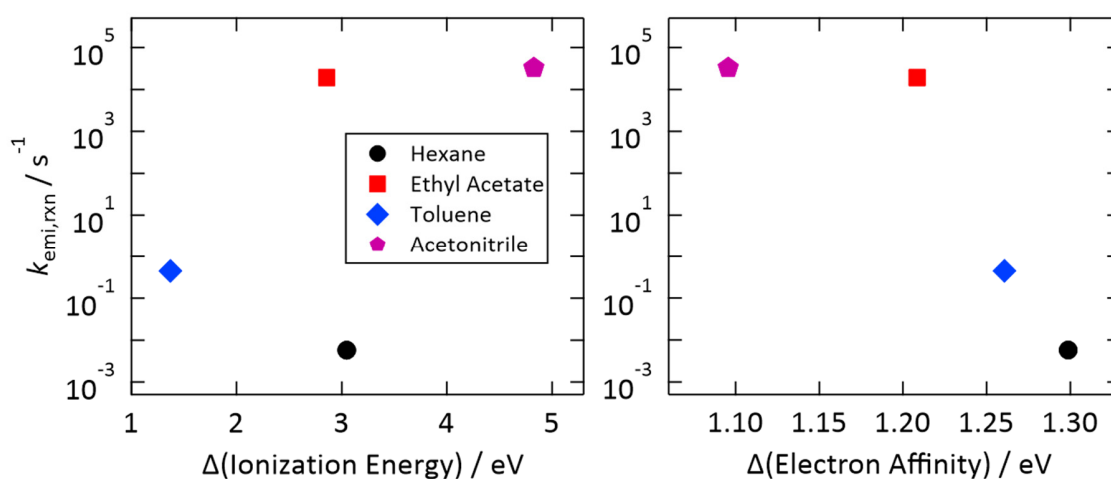

Figure S15. Reaction rates between the T_1 state of **2** and the solvents obtained from the fittings shown in Fig. 4c of the main text plotted against the difference between the ionization energies of **2** and the solvents (left) and the difference between the electron affinities of **2** and the solvents (right).

References

[S1] Y. Murakami, *Chem. Phys. Lett.*, 2011, **516**, 56−61.

[S2] Y. Murakami, H. Kikuchi and A. Kawai, *J. Phys. Chem. B.*, 2013, **117**, 2487−2494.

[S3] Y. Murakami, H. Kikuchi and A. Kawai, *J. Phys. Chem. B.*, 2013, **117**, 5180−5187.

[S4] Y. Murakami, T. Ito and A. Kawai, *J. Phys. Chem. B*, 2014, **118**, 14442−14451.

[S5] T. N. Singh-Rachford and F. Castellano, *J. Phys. Chem. A*, 2009, **113**, 5912–5917.

[S6] P. B. Merkel and J. P. Dinnocenzo, *J. Lumin.*, 2009, **129**, 303–306.

[S7] M. Majek, U. Faltermeier, B. Dick, R. Pérez-Ruiz and A. J. Wangelin, *Chem. Eur. J.*, 2015, **21**, 15496–15501.

[S8] V. Gray, P. Xia, Z. Huang, E. Moses, A. Fast, D. A. Fishman, V. I. Vullev, M. Abrahamsson, K. Moth-Poulsen and M. L. Tang, *Chem. Sci.*, 2017, **8**, 5488–5496.

[S9] M. Barawi, F. Fresno, R. Pérez-Ruiz and V. A. de la Peña O'Shea, *ACS Appl. Energy Mater.*, 2019, **2**, 207–211.

[S10] S. He, X. Luo, X. Liu, Y. Li and K. Wu, *J. Phys. Chem. Lett.*, 2019, **10**, 5036–5040.

[S11] H. L. Lee, M. S. Lee, H. Park, W. S. Han and J. H. Kim, *Korean J. Chem. Eng.*, 2019, **36**, 1791–1798.

[S12] C. E. McCusker and F. N. Castellano, *Top. Curr. Chem. (Z)*, 2016, **374**, 175−199.

[S13] *Wolfram|Alpha*, https://www.wolframalpha.com/.